Opto-Electronic Advances

Original Article

2019, Vol. 2, No. 8

DOI: 10.29026/oea.2019.190003

Ionization behavior and dynamics of picosecond laser filamentation in sapphire

Amina[1,2], Lingfei Ji[1,2]*, Tianyang Yan[1,2] and Rui Ma[1,2]

Currently, laser-induced structural modifications in optical materials have been an active field of research. In this paper, we reported structural modifications in the bulk of sapphire due to picosecond (ps) laser filamentation and analyzed the ionization dynamics of the filamentation. Numerical simulations uncovered that the high-intensity ps laser pulses generate plasma through multi-photon and avalanche ionizations that leads to the creation of two distinct types of structural changes in the material. The experimental bulk modifications consist of a void like structures surrounded by cracks which are followed by a submicrometer filamentary track. By increasing laser energy, the length of the damage and filamentary track appeared to increase. In addition, the transverse diameter of the damage zone increased due to the electron plasma produced by avalanche ionizations, but no increase in the filamentary zone diameter was observed with increasing laser energy.

Keywords: structural modifications; sapphire; picosecond laser; filamentation; ionization dynamics

Amina, Ji L F, Yan T Y, Ma R. Ionization behavior and dynamics of picosecond laser filamentation in sapphire. *Opto-Electron Adv* **2**, 190003 (2019).

Introduction

Over the past several decades, ultrafast laser pulses have been used for the precise and highly localized modification in various optical materials. These permanent structural modifications can be used for the development of three-dimensional integrated optical devices[1–5]. In high band gap transparent materials like sapphire, linear absorption of laser irradiation is limited, thus, nonlinear absorption mechanism is required for a material change to occur. When an ultrafast laser pulse is focused at the focal volume, the intensity becomes sufficient enough ($\sim 10^{13}$ W/cm^2)[6] to induce nonlinear absorption and electrons ionization through multiphoton ionization (MPI) followed by avalanche ionization. As a result, significant plasma density is generated, resulting in free-carrier absorption and impact ionization which counter balances the self-focusing effect. Thus, the change in the material structure occurs as a result of the dynamical balance between self-focusing due to the nonlinear Kerr effect and self-defocusing associated with the plasma formation which is called filamentation[1–3,6–11]. The resulted material structural changes are the visible record of pulse plasma interaction. While using ultrafast laser pulses, it is essential to understand and control the initial laser-matter interaction and resulting free electrons generation for the development of new broad and promising applications.

Numerous studies have analyzed surface and subsurface optical damages and to interpret the results, a wide variety of computer simulations has been applied. Gulley et al.[12] performed simulations to model laser-induced plasma generation in bulk fused silica for single and different-frequency multi-pulse systems. A plasma density generated by 50 fs, 267 nm pulse followed by more energetic 150 fs, 800 nm pulse was predicted to two orders of magnitude greater than either pulse generated alone. The simulation model further demonstrated that the strong pulse chirps generated naturally during nonlinear propagation lead to the ionization dynamics that cannot be captured by standard monochromatic treatment of laser-induced plasma formation. Thus, the proposed model provided a practical framework for the laser-material interactions and a better insight into the physics of the intense ultrafast laser induced ionization[13]. Stuart et al.[14] have shown that if the threshold fluence of a material is below or of the order of 0.2 J·cm^{-2}, photoionization is

[1]Institute of Laser Engineering, Beijing University of Technology, Beijing 100124, China; [2]Key Laboratory of Trans-scale Laser Manufacturing Technology, Ministry of Education, Beijing 100124, China.

*Correspondence : L F Ji, E-mail: ncltji@bjut.edu.cn

Received: 16 February 2019; Accepted: 2 March 2019; Published: 16 August 2019

almost completely responsible for the material optical breakdown regardless of the pulse duration. This was theoretically confirmed by comparing the laser induced ionization mechanism in fused silica and Gallium Arsenide (GaAs) with the band gap 9 and 1.42 eV respectively[15]. For 800 nm wavelength laser pulses, decrease in the pulse duration from 300 fs to 50 fs results a decrease in electron density contribution due to avalanche ionization by 20 million times the photoionization density in fused silica. However, avalanche ionization is a non factor in total electron density growth, when GaAs is irradiated by 1 ps and 50 fs laser pulses with the same 800 nm wavelength.

In the above study, Keldysh photoionization rate theory[14] for solids was used to perform the simulations, which provided a good agreement with experiments of ultrashort laser pulse propagation in fused silica[15,16] and GaAs[15]. However, analyzing the ionization dynamics and resulting damage mechanism in sapphire remains a challenge due to its hardness and wide band gap[16,17]. In addition, nonlinear laser absorption and filamentation in sapphire are still very poorly investigated topics, especially concerning the dynamics of electron density and breakdown behavior under high-intense ultrafast laser pulses. There seems to be little research work on sapphire, and only the mechanism of multiphoton absorption is theoretically described[18,19]. Among these, DeSalvo et al.[18] first determined the multiphoton absorption coefficient by using Z-scan technique and then measured nonlinear refractive index refractive dispersion through Kramers-Kronig transformation. Moreover, multiphoton absorption theory in sapphire has been discussed in details in the frame work of time-dependent *N*th order perturbation theory[19]. However, Keldysh theory is more general, non-perturbative theory that can be used for arbitrarily large field intensities[13,15,19]. Therefore, it is of great significance to better understand the phenomenon of electron density dynamics in sapphire from both theoretical and experimental aspects.

In this paper we discussed electron density growth by implementing Keldysh theory in high power picosecond laser irradiated sapphire. A systematic study has been realized through the variation of the incident laser energy. Furthermore, on the basis of Keldysh theory, the estimated laser pulse induced electron density under our experimental conditions is interestingly far greater than the critical density required to produce laser-induced breakdown in sapphire. Therefore, damages were found, when sapphire was irradiated experimentally under the same theoretical parameters. Besides, we have also observed that the electron density and length of the filament increases almost linearly with input laser energy.

Experimental procedure

A picosecond laser system (Edgewave PX-400, Germany) delivering 10 ps duration pulses at 1064 nm and pulse repetition rate of 300 kHz was used to carry out the experiments. A schematic drawing of the experimental setup used in our experiment is shown in Fig. 1. The pulse energy of the Gaussian-shaped beam was adjusted to between 87 μJ and 107 μJ. The beam with a focal spot diameter of ~10 μm (measured by D2 method[20]) was focused 1 mm beneath the front surface of the sample. Sapphire crystal plate of 2 mm thickness was used in the experiments. The work area was monitored using a CCD camera. Afterwards, the filamentary morphology at different pulse energies was analyzed using a polarizer optical confocal microscope (Leica DM6M). To support out the experiments, numerical simulations of the electron density growth in sapphire were conducted by using Keldysh theory[21], in which, the significance and behavior of the photoionization and avalanche ionization along the propagation were described for the given experimental parameters using MATLAB scripts.

Results and discussion

By employing the phenomenon of filamentation, the use

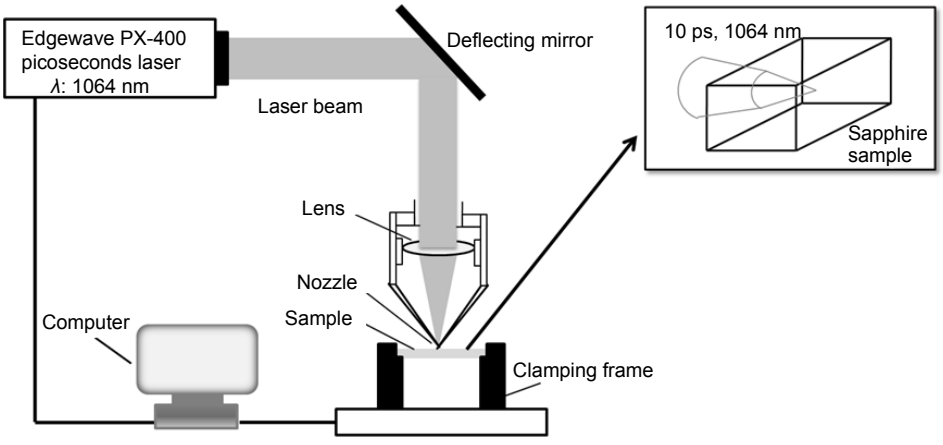

Fig. 1 | Schematic diagram of the experimental setup.

of high peak intensities of ultrafast laser provides a unique ability to induce a confined and non-thermal damage mechanism in the bulk of transparent materials. When the laser power exceeds the critical power of self-focusing in sapphire, filamentary propagation of the laser beam is observed. For Gaussian beam, the critical power for self-focusing was calculated using the relation[1,3,22,23] $P_{cr} = 3.77\lambda^2/8\pi n_0 n_2$, where λ is the laser wavelength, n_0 and n_2 are the linear and nonlinear refractive indices respectively. For sapphire, the critical power at the wavelength 1064 nm is calculated to be 2.81 MW with linear and nonlinear index values of 1.78 and 3.40×10^{-20} m^2/W, respectively[18]. The corresponding critical energy at a pulse duration of 10 ps can be calculated as[24], $E_{cr} \approx \sqrt{\pi/2}\,\tau P_{cr} = 35\,\mu J$, where τ is the pulse duration. A picosecond (ps) laser system operating at the 1064 nm wavelength with pulse repetition rate of 300 kHz has the input energy values of 87 μJ, 93 μJ, 100 μJ and 107 μJ in the experiments. Therefore self-focusing occurred in sapphire because the values of laser powers and the corresponding energy chosen in our experiments are all well above the threshold needed for the self-focusing.

When an optical material is subject to an intense electromagnetic wave, free-carrier generation occurs due to photoionization or electron impact ionization and subsequent avalanching. Various laser and material parameters are used to determine the relative role of each process contributing to the material breakdown. To demonstrate this in sapphire, the estimated values of the photoionization and avalanche ionization electron density achieved along the propagation for our experimental parameters in time are shown in Fig. 2(b) with the corresponding laser intensities shown in Fig. 2(a). The time scale given in the intensity-time graph is in ps and the intensity interval is given in both the positive and negative side of such small interval of time in order to cover the wavelength (vibrational mode) of laser. Figure 2(b) shows the numerical simulations of electron density growth obtained for 87 μJ, 93 μJ, 100 μJ and 107 μJ laser energies by using Keldysh theory as described in Ref.[13,15,21,23,25] Primarily, at the peak of the pulse, high-intensity photon flux leads to the generation of free electrons by photoionization process. However photoionization becomes less important as the peak passes and electrons excited at the peak serve as seeds for avalanche ionization. Solid lines correspond to total electron density, while dotted lines correspond to photoionization electron density profiles. Based on the simulation, it is concluded that avalanche ionization plays an increasingly significant role in the electron density growth with increasing energy and the maximal electron density values obtained is in the range of approximately 10^{49}–10^{61} cm^{-3}, while the value photoionization rate in the focal area is in the range 10^{10}–10^{11} cm^{-3}. These values are approximately 10^{45} orders of magnitude greater in avalanche ionization than what have been obtained in photoionization electron density in the theoretical model. Since avalanche ionization strongly depends on the laser intensity, laser intensity was observed to be higher at high laser energy as described in Fig. 2(a). Therefore, electron density growth with laser energy is greater in avalanche ionization as compared to photoionization, as shown in Fig. 2(c) in a more clear way. However photoionization is the key process to material breakdown whether providing critical electron density directly by itself or by seed electrons necessary for avalanche breakdown to occur.

Photoionization refers to the direct excitation of electrons by laser field. Depending on the intensity and frequency of the incident pulse, multiphoton and tunneling are the two regimes of photoionization. Whether the ionization process occurs through multiphoton or tunneling regime, was remarkably described by Keldysh adiabatic parameter γ[15]:

$$\gamma = \frac{\omega}{e}\sqrt{\frac{m_e c n \varepsilon_0 E_g}{I}}\quad , \tag{1}$$

where ω is the laser frequency, e is the electron charge, m_e is the electron effective mass, c is the speed of light, n is the refractive index of material, ε_0 is the permittivity of free space, E_g is the band gap, and I is peak intensity of laser. When Keldysh parameter γ falls below 1.5, photoionization corresponds to the tunneling ionization regime. On the other hand, γ being above 1.5 corresponds

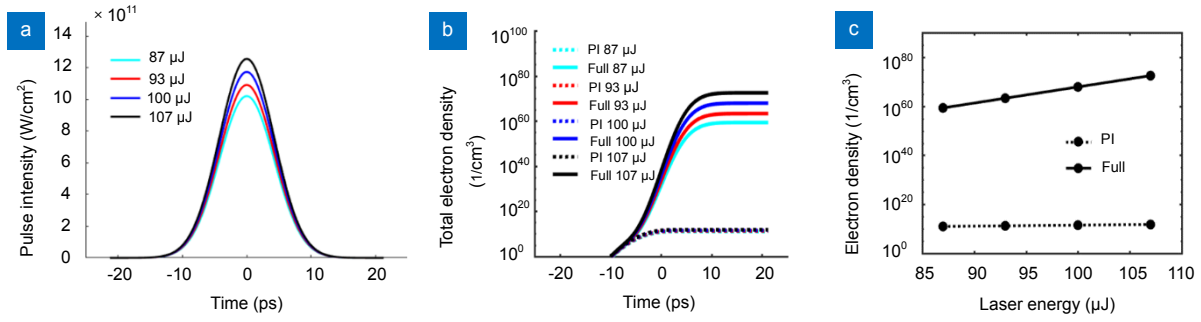

Fig. 2 | (**a**) Laser beam intensity profiles simulation for the energies 87 μJ, 93 μJ, 100 μJ and 107 μJ. (**b**) Simulation of the significant role avalanche plays after photoionization (PI) introduces "seed" electrons in sapphire when irradiated with different laser energies. (**c**) Full and PI electron densities as a function of laser energy.

to the MPI regime where electrons can be considered to have time for many oscillations in the binding potential before being ionized. In addition, the intermediate regime where both tunneling and MPI contribute, occurs when the parameter is near or equal to 1.5. Figure 3(a) describes total photoionization rate, significance and behavior of the individual roles of MPI and tunneling ionization versus intensity using MATLAB scripts. The solid cyan line in Fig. 3(a) corresponds to the total photoionization rate. The blue and red lines represent MPI and tunneling rates respectively. Figures 3(b) and 3(c) give more clear explanation of the transition regime from MPI to tunneling ionization relationship with Keldysh parameter. It can be seen in Figs. 3(b) and 3(c) that the full rate only agrees with MPI rate for γ >1.5 and solely with tunneling rate for γ < 1.5. Tunneling and MPI rates overlap each other at $\gamma \approx 1.5$. It is important to note that the abrupt changes in the MPI process causes step like behavior in the full rate photoionization. This is because the effective band gap increases as the laser intensity increases, thereby increasing the number of photons required to ionize electrons, more clearly shown in Figs. 4(a) and 4(b). At high laser intensities greater than 10^{12} W/cm^2, the effective band-gap starts increasing from 10 eV as shown in Fig. 4(a). Consequently, the number of photons required for MPI process in sapphire increases from 9 to 10 photon process and so on (Fig. 4(b)).

In order to investigate the influence of laser pulse energy on free-carrier generation and filamentation, various tracks induced in sapphire sample with input laser energies of 87 μJ, 93 μJ, 100 μJ and 107 μJ were investigated. This energy range was well above the pulse energy corresponding to the critical power for self-focusing in sapphire (35 μJ) and resulting in strong modification of the beam propagation. The resulted microscopic photographs corresponding to the structural modification regions as a function of the input laser energy are shown in Fig. 5(a). The laser beam propagates from the right to left of the images. As long as the pulse peak power remains above the critical power P_{cr}, there would be a chance for the diverging beam to refocus again one or more times right after the geometrical focus.

A closer look at the image (Fig. 5(a)) shows that the length of the modified tracks is more than 2 mm, which starts after few-micrometer propagation in the sample due to high transmission wavelength range and low laser fluence of the material. As the input laser energy increases from 87 μJ to 107 μJ, the total length of the track expands from 2.2 mm to 2.3 mm as indicated in Fig. 5(b). Moreover, one can clearly observe in Fig. 5(a) that each irradiated track consists of a slightly elliptical irregular morphology followed by a narrow filamentary track of constant diameter in the direction of laser beam propagation.

As the laser beam contracts spatially at the focal region, its intensity rises and becomes sufficient enough (~10^{13} W/cm^2)[6] to ionize electrons through multi-photon absorption followed by avalanche ionization due to which a

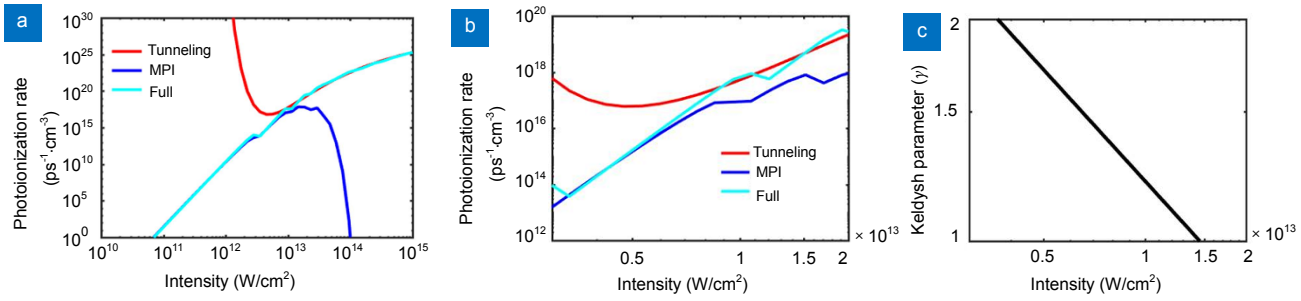

Fig. 3 | (**a**) Total photoionization, MPI and tunneling ionization rate as a function of laser intensity in sapphire. (**b**) Enlarge image where MPI and tunneling ionization rate overlap at a Keldysh parameter of about 1.5. (**c**) Keldysh parameter as a function of laser intensity in sapphire.

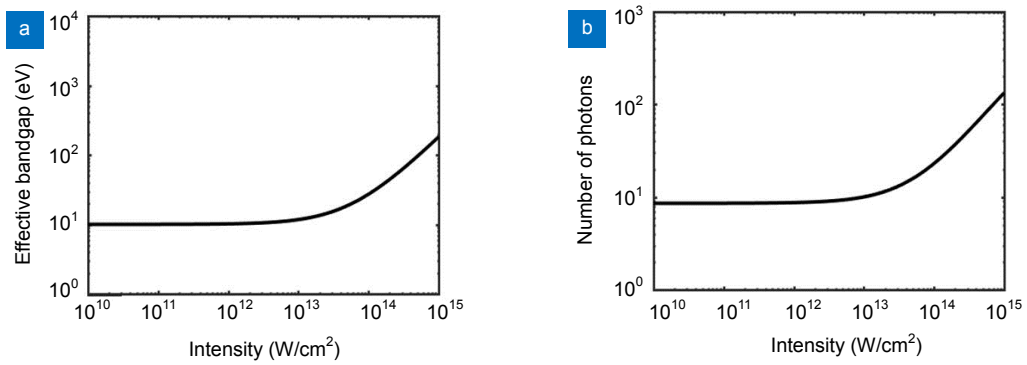

Fig. 4 | (a) Effective bandgap and (b) number of photons required for MPI process as a function of laser intensity in sapphire.

localized plasma is formed at the focal region. As the temperature of the exposed region increases further, plasma causes a large charge separation resulting in high pressure. As a result, the generation of shock waves occurs which carries matter and energy away from the focal region, compressing the surrounding material and leaving a hollow central region termed as void. Hence, the observed structural modifications consisted of an irreversible well-localized central damage surrounded by an extended volume of nonpermanent smooth refractive index changes in the form of cracks, which is consistent with Ref.[17] Note that the strong damage occurred right before the geometrical focus in which laser scattered signal extended over the region between the self and geometrical foci. These results indicated that the on-axis plasma density near the geometrical focus would be higher than that at the nonlinear self-focus. Earlier studies have shown that the electron density level is directly related to the damage produced in the bulk of the transparent solid, and its limit was found to be in the range 10^{21} electrons·cm^{-3}.[15] Numerically, these values of electron density can be attained only through electron avalanches. As shown in Fig. 2, avalanche ionization in the electron density growth along the filament is higher than that of photoionization rate. Thus, electron avalanche is shown to play an important role for bulk material damage in this case.

Figure 5(a) further revealed that an increase in the laser energy has an impact on the formation and characteristics of damage track in sapphire. With increase in the laser energy, the leading point of the damage track moves towards the laser source direction, resulting in an increase in the length of damage track, as shown in Figs. 5(a) and 5(b). It is due to the fact that the increase in the laser energy causes self-focusing to appear earlier which is consistent with the previous work for fused silica[22]. This energy-dependent considerable shift of the linear focus, owing to self-focusing, toward the laser source was measured and plotted in Fig. 5(b) as the distance between sample surface and starting position of the damage track. Each pulse self-focuses at different point due to the difference in laser energy, as a result, the start-up position has changed. This phenomenon was the major reason for the observed increase in the damage zone length with increase in laser energy.

Numerically, this behavior can be well described qualitatively by a well-known Marburger formula, that is, a collimated Gaussian laser beam with a radius a (at $1/e^2$ intensity), wave number k, and instantaneous power P_{in}, self-focuses at a point of collapse L_c, measured from the sample input surface[23,26,27]:

$$L_c = \frac{0.367ka^2}{\sqrt{\left[\sqrt{P_{in}/P_{cr}} - 0.852\right]^2 - 0.0219}}, \qquad (2)$$

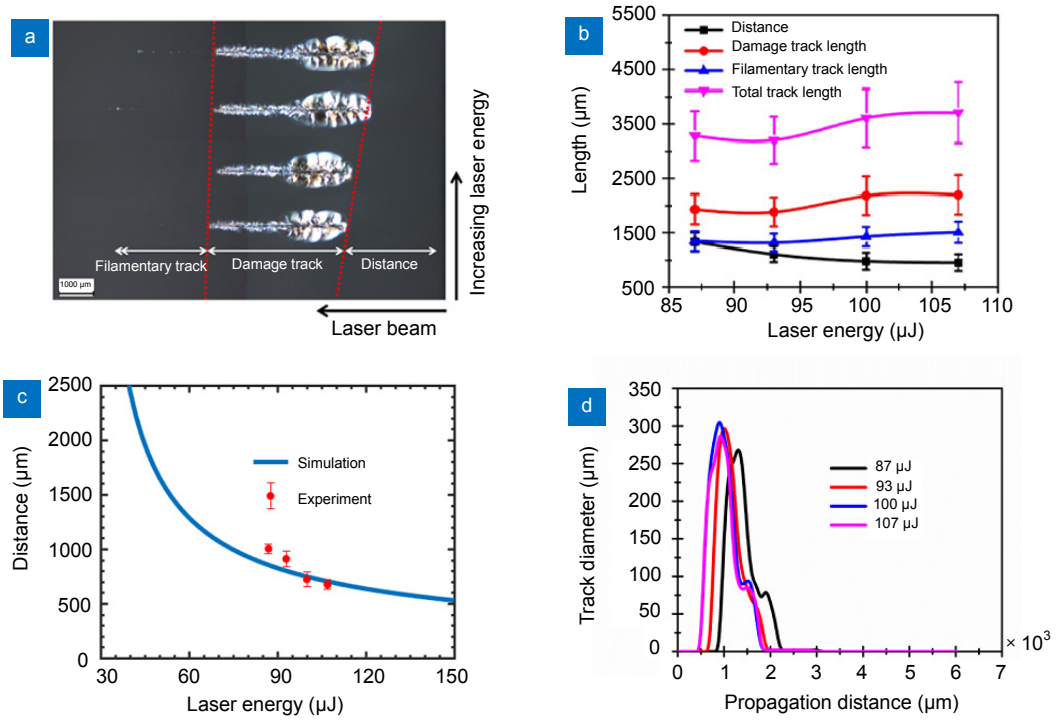

Fig. 5 | (**a**) Microscopic images of the laser induced tracks obtained at laser energies 87 μJ, 93 μJ, 100 μJ and 107 μJ (bottom to top) and 12000 number of pulses. (**b**) Plot of the distance between sample surface and starting point of the modified track, and length of total track, damage zone and filamentary track as a function of laser energy. (**c**) Comparison between the measured (●) and calculated (——) distance between sample surface and the starting point of the modified area versus pulse energy. (**d**) Spatial profile of the laser induced tracks diameter along the propagation path for different energies.

where P_{cr} is the critical power for self-focusing in the medium. Here, the instantaneous peak power is given by $P_{in} = E_{in}/\tau$, where E_{in} is the input energy and τ is the laser pulse width. In case of focusing with an external lens of focal length f, the position of the self-focus shifts to $L_f = L_c f/ (L_c + f)$. In sapphire, simulation results of the point of collapse L_f, with experimental data are illustrated in Fig. 5(c). These numerical simulation results are in agreement with experimentally measured values, showing that in sapphire sample the damage track starts shifting towards the sample input face with increasing input laser energy. Moreover, the modified tracks show that the damage tracks have become more pronounced in the radial direction as well with increasing laser energy.

To further characterize its spatial distribution, the diameter of the modified track profiles was measured and plotted as the function of the propagation distance for various laser pulse energies as shown in Fig. 5(d). Transversely, the size of the modification tracks appears to increase firstly due to the electron plasma produced by the pulse as it propagated. With pulse energy at 100 μJ, the crack diameter expands up to 300 μm. A reasonable explanation is that the damage channel diameter is enlarged by cracks due to high plasma density formation around the geometrical focus. However, at later the diameter of the laser-induced damage tracks dropped sharply where it remains constant till the end of the track. As shown in Fig. 5(a), the narrow filamentary track of constant diameter ~2 μm formed along the laser path as a result of nonlinear laser beam focusing and defocusing is resulted from the stable incident pulse energy and sensitive to the energy. At high laser energies, increase in length of the filamentary track was observed, as illustrated in Figs. 5(a) and 5(b). Length of the filamentary track increases in the laser propagation direction, when laser pulse energy increases and a maximum of 1036 μm length with 2 μm diameter was observed at energy 107 μJ.

Figure 2 illustrates the dependence of the plasma density along the filament and around the geometrical focus on laser intensity and pulse energy. Simulation model based on the Keldysh theory shown in Fig. 2 and the experimental observations (Fig. 5) lead to similar conclusion and therefore the structural damage near the geometrical focus is caused by avalanche ionization due to a large excess of the pulse power over P_{cr}. Furthermore, inspection of the modified zones in Fig. 5(a) brings to light that for the parameters chosen in our experiments, the total length of the track, damage track and filamentary track increases with input energy as illustrated Fig 5(b).

Conclusions

This work aimed to investigate the ionization mechanism of picosecond laser induced filamentation in sapphire which is with high refractive index. Experimentally, by tightly focusing laser pulses, free carriers generation and plasma formation led to two types of structural changes in the bulk of sapphire material namely: void like structure surrounded by cracks and filamentary tracks. By increasing laser energy, the diameter of the damaged zone has increased due to the electron plasma produced by avalanche ionizations, while the diameter of the filamentary track remained unchanged at 2 μm. Based on Keldysh theory, numerical simulations have confirmed the significant increase of the electron density growth with increasing laser energies. However, the increase rate was observed to be higher in avalanche ionization as compared to multiphoton ionization. Thus, avalanche ionization mechanism was found to dominate over multiphoton ionization. Furthermore, the length of the damage zone and filamentary track was found to increase with increasing laser input energy, and a maximum filamentary track length of about 1036 μm was observed at 107 μJ energy.

References

1. Ahmed F, Ahsan M S, Lee M S, Jun M B G. Near-field modification of femtosecond laser beam to enhance single-shot pulse filamentation in glass medium. *Appl Phys A* **114**, 1161–1165 (2014).
2. Lanier T E, Gulley J R. Nonlinear space-time focusing and filamentation of annular femtosecond pulses in dielectrics. *J Opt Soc Am B* **33**, 292–301 (2016).
3. Masselin P, le Coq D, Bychkov E, Lépine E, Lin C *et al*. Laser filamentation in chalcogenide glass. *Proc SPIE* **7993**, 79931B (2011).
4. Yang Q, Ji L F, Xu B, Yan T Y, Wang W H *et al*. Picosecond laser microfabrication of infrared antireflective functional surface on As_2Se_3 glass. *Opto-Electron Eng* **44**, 1200–1209 (2017).
5. Zhou R, Lin S D, Ding Y, Yang H, Ong K *et al*. Enhancement of laser ablation via interacting spatial double‐pulse effect. *Opto-Electron Adv* **1**, 180014 (2018).
6. Couairon A, Mysyrowicz A. Femtosecond filamentation in transparent media. *Phys Rep* **441**, 47–189 (2007).
7. Galinis J, Tamošauskas G, Gražulevičiūtė I, Keblytė V, Jukna V *et al*. Filamentation and supercontinuum generation in solid-state dielectric media with picosecond laser pulses. *Phys Rev A* **92**, 1–5 (2015).
8. Liu Z, Lu X, Liu Q, Sun S, Li L *et al*. Ultraviolet conical emission produced by high-power femtosecond laser pulse in transparent media. *Appl Phys B* **108**, 493–500 (2012).
9. Durand M, Jarnac A, Houard A, Liu Y, Grabielle S *et al*. Self-guided propagation of ultrashort laser pulses in the anomalous dispersion region of transparent solids: a new regime of filamentation. *Phys Rev Lett* **110**, 115003 (2013).
10. Javaux Léger C, Mishchik K, Dematteo-Caulier O, Skupin S, Chimier B *et al*. Effects of burst mode on transparent materials processing. *Proc SPIE* **9351**, 93510M (2015).
11. Ji L F, Amina, Yan T Y, Wang W H, Wang T R *et al*. Research progress of ultrafast laser industrial applications based on filamentation. *Opto-Electron Eng* **44**, 851–861 (2017).
12. Gulley J R, Liao J X, Lanier T E. Plasma generation by ultrashort multi-chromatic pulses during nonlinear propagation.

Proc SPIE **8972**, 89720T (2014).
13. Gulley J R, Lanier T E. Model for ultrashort laser pulse-induced ionization dynamics in transparent solids. *Phys Rev B* **90**, 155119 (2014).
14. Stuart B C, Feit M D, Herman S, Rubenchik A M, Shore B W *et al*. Optical ablation by high-power short-pulse lasers. *J Opt Soc Am B* **13**, 459–468 (1996).
15. Ferris C. Theoretical modeling of laser-induced absorption phenomena in optical materials (University of Nebraska, Lincoln, Nebraska, 2014).
16. Wang C W, Zhao Q Z, Qian J, Li Y B, Wang G D *et al*. Propagation of focused ultrashort pulse laser during micromachining of sapphire. *Proc SPIE* **9532**, 95320O (2015).
17. Benayas A, Jaque D, McMillen B, Chen K P. Thermal stability of microstructural and optical modifications induced in sapphire by ultrafast laser filamentation. *J Appl Phys* **107**, 033522 (2010).
18. DeSalvo R, Said A A, Hagan D J, Van Stryland E W, Sheik-Bahae M. Infrared to ultraviolet measurements of two-photon absorption and n_2 in wide bandgap solids. *IEEE J Quantum Electron* **32**, 1324–1333 (1996).
19. Arola E. Theoretical studies on multiphoton absorption of ultrashort laser pulses in sapphire. *IEEE J Quantum Electron* **50**, 709–720 (2014).
20. Liu J M. Simple technique for measurements of pulsed Gaussian-beam spot sizes. *Opt Express* **7**, 196–198 (1982).
21. Keldysh L V. Ionization in the field of a strong electromagnetic wave. *Sov Phys JETP* **20**, 1307–1314 (1965).
22. Papazoglou D G, Zergioti I, Tzortzakis S, Sgouros G, Maravelias G *et al*. Sub-picosecond ultraviolet laser filamentation-induced bulk modifications in fused silica. *Appl Phys A* **81**, 241–244 (2005).
23. Lotti A. Pulse shaping and ultrashort laser pulse filamentation for applications in extreme nonlinear optics (University of Insubria, Insubria, 2012).
24. Couairon A, Sudrie L, Franco M, Prade B, Mysyrowicz A. Filamentation and damage in fused silica induced by tightly focused femtosecond laser pulses. *Phys Rev B* **71**, 125435 (2005).
25. Wu M T, Guo B, Zhao Q L, Fan R W, Dong Z W *et al*. The influence of the focus position on laser machining and laser micro-structuring monocrystalline diamond surface. *Opt Lasers Eng* **105**, 60–67 (2018).
26. Saliminia A, Nguyen N T, Chin S L, Vallée R. The influence of self-focusing and filamentation on refractive index modifications in fused silica using intense femtosecond pulses. *Opt Commun* **241**, 529–538 (2004).
27. Liao M S, Gao W Q, Cheng T L, Duan Z C, Xue X J *et al*. Filamentation and supercontinuum generation in tellurite glass. *Proc SPIE* **8621**, 86211O (2013).

Acknowledgements

This work is supported by National Natural Science Foundation of China (51575013, 51275011) and National Key R & D Program of China (2018 YFB1107500)

Competing interests

The authors declare no competing financial interests.